ELSEVIER

Earth and Planetary Science Letters 143 (1996) 183–195

EPSL

Comparisons between the rift systems of East Africa, Earth and Beta Regio, Venus

Adrian Foster *, Francis Nimmo [1]

Bullard Laboratories, University of Cambridge, Madingley Rise, Cambridge, CB3 0EZ, UK

Received 20 October 1995; accepted 23 July 1996

Abstract

The rift systems of southern East Africa and Beta Regio, Venus are similar in a number of ways. The rifted East African and Venusian lithospheres have effective elastic thicknesses of ~30 km, suggesting that both lithospheres maintain significant flexural strength during rifting. Both rift systems have maximum fault segment lengths of ~100 km. The effective elastic thickness and maximum fault segment length of both rifts are greater than those seen in many other active extensional regions on Earth, despite the high surface temperatures on Venus. We suggest that the southern East African and Venusian elastic thicknesses and maximum fault segment lengths are due to stronger lithosphere. The rift systems differ in the maximum width of their half graben. East African half grabens are up to ~50 km wide, whilst those on Venus are up to ~150 km wide. To support the topography associated with such half grabens requires shear stresses to act on the bounding faults. In East Africa the greater elastic thickness (compared to most other terrestrial extensional regions) means that wide half grabens can form without requiring the shear stresses acting on the bounding faults to be greater than the ~1–10 MPa (10–100 bars) stress drop typically seen in earthquakes. However, on Venus the absence of sediment infill, greater widths and larger effective topographic steps of the half grabens require shear stresses of up to ~80 MPa (800 bars) to act on the bounding faults. This difference is significant; Venusian faults must be stronger than those on Earth.

Keywords: East African Rift; Beta Regio; rifting; faults

1. Introduction

Earth and Venus are approximately the same size (1° of latitude is ~111 km on Earth and ~106 km on Venus), and both planets have well-developed rift systems. When viewed at a regional scale the geometry of the fault systems bounding the rifts of East Africa and Beta Regio, Venus are similar (compare the morphology of Fig. 1a and b). In this paper we present new data from Beta Regio, and compare the two rift systems in terms of their effective elastic thickness (T_e), maximum fault segment lengths and maximum rift basin widths. These parameters are used to characterise extensional regions on Earth, and may be related; in general extensional regions with a greater T_e are characterised by longer faults and wider basins [1–5].

The East African Rift System runs from the Red Sea/Gulf of Aden/Afar triple junction in the north to offshore Tanzania and Mozambique in the south.

* Corresponding author. E-mail: foster@esc.cam.ac.uk
[1] E-mail: nimmo@esc.cam.ac.uk

PII S0012-821X(96)00146-X

The rift bifurcates around Lake Victoria into the Eastern and Western branches (Fig. 1a), which lie mainly in Archean and Proterozoic basement. Volcanism began at ~ 30 Ma in the north [6] and at ~ 9 Ma in the south [7]. Cumulative extension across most of the rift system is small. Estimates of total extension based on reconstructions of surface fault geometries in the Western branch of the rift are ~ 3–4 km, but may be up to ~ 10 km in the wide basins of Lake Tanganyika and Lake Malawi [8,9]. Current plate models suggest approximately east–west extension across the rift at a rate of ~ 3–5 mm/year [10]. The broad topographic plateaux of East Africa (Fig. 1a) and Afar are characterised by long-wavelength negative Bouguer gravity anomalies [11]. These anomalies are attributed to the presence of low density asthenosphere beneath the plateaux. A convecting region within the asthenosphere has been proposed to explain the dynamic component of support for the plateaux [12].

Several people have reported earthquake centroid depths in East Africa which are deeper than the 5–15 km range typical of most other regions of active continental extension (e.g. Greece, Turkey, western USA, Tibet, SW China, Italy, Suez) [2,13–15]. The Baikal Rift is similar to East Africa in also having deeper earthquakes [16]. Most of the deep East African earthquakes lie away from the topographic expression of the rift, and all lie towards the southern end of the rift system. Crustal thicknesses in most of the epicentral areas are poorly constrained, but are probably in the range 30–40 km [17]. Hence, we cannot be sure whether centroid depths in the range of 25–35 km lie in the crust or in the upper mantle. These centroid depths suggest that the seismogenic thickness in parts of East Africa is 30–35 km,

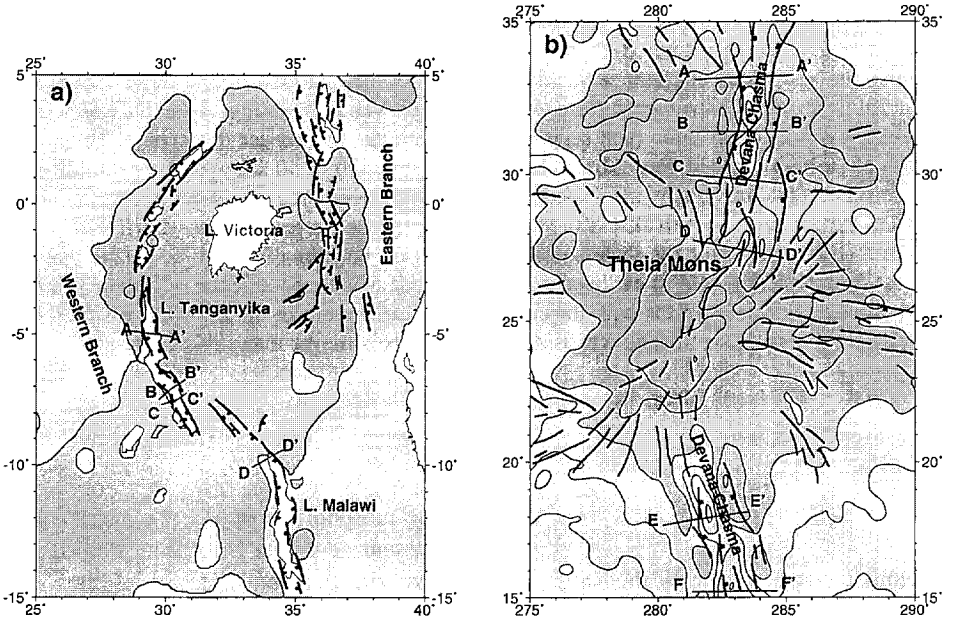

Fig. 1. Mercator projection regional maps of the southern East African and Beta Regio rift systems showing long-wavelength topography (contoured at 1000 m intervals) and border fault systems (faults have ticks on downthrown side). Both rift systems lie on top of broad topographic domes. Both maps are drawn to the same scale (1° of latitude is ~ 111 km on Earth and ~ 106 km on Venus). (a) The East African Rift System bifurcates around Lake Victoria into the Eastern and Western branches. Topography was produced by applying a 100 km full width median filter to the ETOPO5 dataset, and gridding the output at 5-min intervals. Darker shading indicates topography above 1000 m. Border fault systems taken from [8,9,12,17,29,30,38]. Lines of profiles in Fig. 5 and Fig. 6a are shown. (b) In Beta Regio the rift systems of Devana Chasma radiate out from the volcanic construct of Theia Mons. Border fault systems taken from [19]. The sense of movement across most border faults is unknown. Topography calculated at 0.5 degree intervals from 360th degree and order spherical harmonics using $l = 2$ to 360. Darker shading indicates topography above 2000 m. Lines of profiles in Fig. 6 are shown.

approximately double that found in most other active extensional regions.

Beta Regio (Fig. 1b) is a prominent regional topographic rise in the Northern Hemisphere of Venus. Like the East African and Afar plateaux, it has been identified as a possible plume site on the basis of topography, gravity and radar images [18,19]. At the centre of the region is Theia Mons, a volcanic construct showing lava flows radiating outwards, and occurring at the intersection of several rift valleys. The composition of these flows, and indeed that of the crust of Venus, is uncertain. Of three major element analyses one approximated the composition of a tholeiitic basalt [20]. The most prominent of the rifts, Devana Chasma, runs northwards from Theia Mons for several hundred kilometres into Rhea Mons, a block of probably older, highly deformed and crustally thickened terrain (tessera). By measuring the width of imaged fault scarps across the rift, and assuming an initial fault plane dip of 45–60° [1], the total extension across the rift can be estimated at 20 ± 10 km, although the age and duration of the rifting are not constrained.

2. Effective elastic thickness estimates

In recent years many studies have estimated the effective elastic thickness (T_e) of the continental lithosphere to be between 5 and 110 km ([21,22], and references therein). It is clear that the strength of the continental lithosphere is somehow controlled by its thermal state [23], although the large variations in T_e have not been satisfactorily explained. However, in regions of continental extension such as the western USA, the North Sea and Greece, T_e is consistently 10–15 km or less ([21,22], and references therein, [24–26]).

The rifting and volcanism associated with the East African Rift System produce topography and gravity signals which have been used to estimate the T_e of the East African lithosphere. By using the wavelength dependence of the coherence between the topography and the Bouguer gravity anomaly [27] Bechtel et al. [28] and Ebinger et al. [12] obtained values of 25 km and 27–31 km, respectively, for the Eastern branch. Using the same method Ebinger et al. [12] estimated T_e to be 32–36 km in the Western branch. Ebinger et al. [29] and Upcott et al. [30] used forward modelling of free air gravity anomalies to estimate a T_e of 17–38 km and 25 ± 5 km, respectively, in the Western branch.

These high values of effective elastic thickness in the southern East African Rift contrast with much lower values (less than 10–15 km) found in many other regions of continental extension elsewhere on Earth (e.g. [21,22] and references therein, [24–26]). This suggests that parts of the uppermost East African lithosphere are stronger than the lithosphere in those other extensional regions. Since the effective elastic thickness of continental lithosphere is probably related to thermal structure [23] we attribute the anomalously high values in the southern East African Rift to the cold (and old) Archean and Proterozoic material being rifted. The occurrence of deep earthquakes within the southern part of the East African Rift System suggests a thicker seismogenic layer, probably because of the nature of the material being rifted [3].

The admittance technique [31] has been used to obtain regional estimates of the elastic thickness of the Venusian lithosphere [32]. An area covering the Beta region (60°S to 60°N and 240°E to 310°E) produced a T_e of ~ 30–35 km, greater than the Venus global average of ~ 20–25 km. Smrekar [33] used spectral methods to estimate a T_e of 25–35 km at Beta Regio and 20–35 km at Atla Regio. Phillips [34] also used spectral methods to obtain a T_e of 40–50 km at Atla Regio.

3. Maximum fault segment lengths

Along-strike segmentation of the border fault systems bounding continental rifts is common, with laterally continuous segments stepping en echelon or changing the polarity of half grabens (e.g. [35,36]). Jackson and White [1] point out the similarity between the maximum segment length of ~ 20–25 km common in many extensional areas and the thickness of the seismogenic upper crust (~ 15 km) or down-dip fault width (~ 20 km) in those areas. They suggest that the maximum length scale of segmentation of the border faults is in some way controlled by the thickness of the seismogenic layer in which they form. The occurrence of deeper earthquakes in parts

of southern East Africa suggests a seismogenic thickness of 30–40 km in those regions; approximately double that seen in most other active continental rifts (e.g. Greece, Turkey, western USA). Hence we may expect East Africa to have individual fault segments with a maximum length scale greater than found elsewhere.

In many parts of East Africa large, high-angle normal fault systems (border fault systems) bound one side of asymmetric basins (half grabens) (e.g. [8]). The other side of such basins consists of a warped margin, often with minor faulting. Individual half grabens in the southern East African Rift are often longer than 100 km (Fig. 1a) (e.g. [8,37,38]). In some places the border fault systems bounding these half grabens consist of several fault segments, with segmentation at a scale much less than 100 km. However, in other places segment lengths of up to 50–100 km have been identified in detailed studies of half grabens and their border fault systems [8,9,39,40]. These long individual border fault segments all occur towards the southern ends of the Eastern and Western branches of the rift, where the seismogenic thickness is 30–35 km. In contrast, maximum fault segment lengths at the northern end of the rift system in Afar, where earthquakes have normal centroid depths, are much less than ~ 30 km. These faults may have superseded older, longer segments [3]. Seismic reflection profiles in the rift lakes of the Western branch suggest that the total

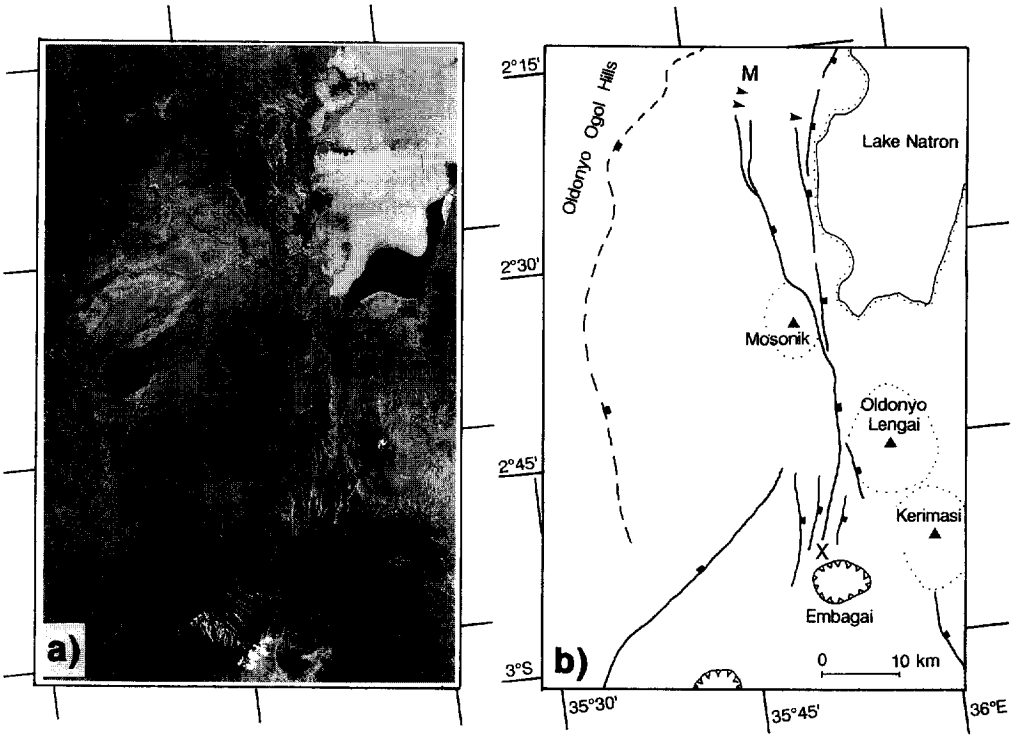

Fig. 2. (a) Landsat TM image of the Embagai/Lake Natron area in northern Tanzania. (b) Summary line drawing of (a) showing the Neogene volcanic centres (solid triangles and dotted outlines) and individual, Pleistocene rift-bounding faults which make up the Natron border fault system (faults have ticks on downthrown side). The long dashed fault bounding the eastern side of the Oldonyo Ogol Hills separates Proterozoic basement from Neogene volcanics and sediments, and is probably no longer active [41]. The Mosonik fault segment runs from the monocline in the north (point *M*) to Embagai crater in the south (point *X*), a distance of ~ 60 km. Faults of this length and longer are found elsewhere in the southern part of the East African Rift System. These faults are much longer than the ~ 20–25 km maximum fault segment lengths seen in other actively extending regions. Displacement across the Mosonik fault segment grows from zero at the monocline (*M*) to at least 600 m (the height of the fault scarp) just south of the Mosonik volcanic centre, and back to zero at Embagai (*X*).

throws across the border faults are up to ~ 7 km [8,9], though the topographic step has been reduced by sedimentation in the hanging wall.

Fig. 2 shows one example of a long fault segment from the southern end of the Eastern branch in northern Tanzania. The Mosonik fault runs from a monocline in the north (point M, Fig. 2) to Embagai crater in the south (point X, Fig. 2) and is a single fault segment whose length is about 60 km. It forms part of the Pleistocene, east-dipping border fault system bounding the western side of the ~ 40 km wide Lake Natron basin. The basin is asymmetric, with its eastern margin being obscured by later volcanism but not being bounded by a border fault system. The heavily dissected fault escarpment to the east of the Oldonyo Ogol Hills is of Pliocene age, and separates Proterozoic basement from the Plio–Pleistocene syn-rift volcanics and sediments [41]. The height of the scarp across the Mosonik fault segment grows from zero at the monocline in the north (point M, Fig. 2) to at least 600 m just south of Mosonik itself, and then decreases southwards to zero at Emgagai crater (point X, Fig. 2). Field studies have shown that the 4 km bend in the fault trace around the Mosonik volcanic centre is not a segment boundary since the fault can be traced continuously around the bend, with a footwall of roughly constant elevation that forms a prominent bench. The displacement across the fault decreases in a regular manner from at least 600 m near the Mosonik volcanic centre to zero at the monocline in the north, and this pattern is not affected by the bend. Such bends in the fault trace are common along the faults bounding the half grabens in northern Tanzania, and

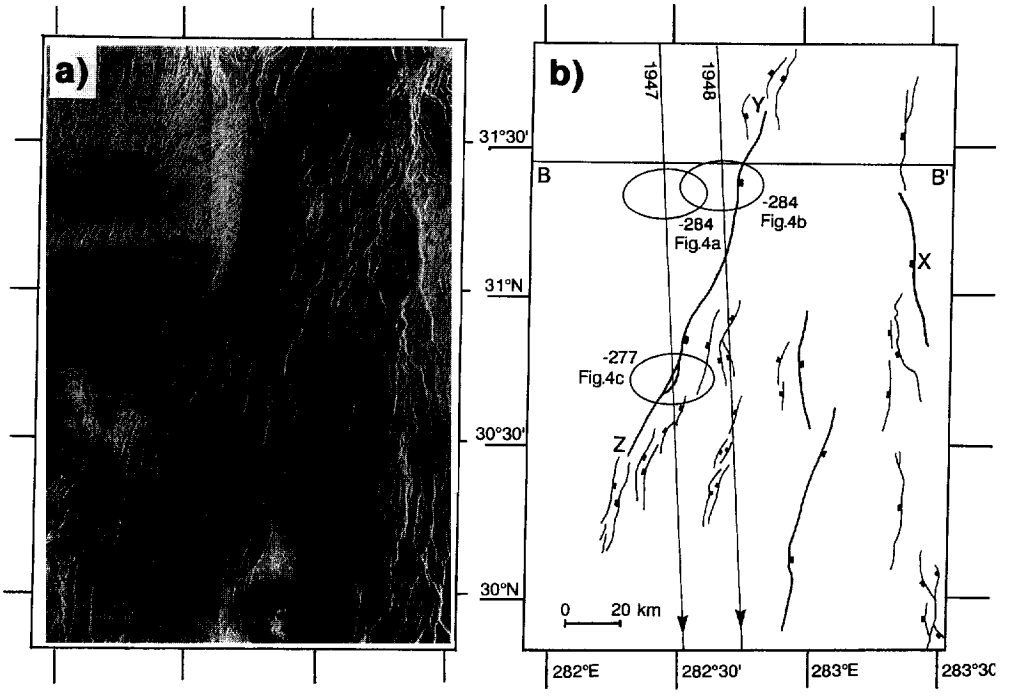

Fig. 3. (a) Part of Magellan SAR image F-MIDR-30N281 showing part of Devana Chasma. Illumination is from the left (west). (b) Line drawing of the area in (a) showing those faults across which a sense of movement can be obtained (thicker pen; ticks on downthrown side). Some smaller faults/lineations are marked (thinner pen). Because the radar is east-looking, dark or shadowed east-dipping faults appear wider than bright west-dipping faults. An east-dipping fault (*Y–Z*) is marked. The fault has zero displacement in the north at point *Y* and runs south to point *Z* where the displacement returns to zero. This fault is ~ 130 km long. *X* marks a large west-dipping fault. The area between these two faults is marked by numerous N–S-trending lineations which may be small fault scarps. Also shown are the line of topographic profile *B–B'* (Fig. 6) and two adjacent groundtracks (*1947* and *1948*) of the Magellan spacecraft (with direction of flight marked). The numbered ellipses on each groundtrack are the individual altimetry footprints whose returns are shown in Fig. 4a, b and c. Each footprint has a 28-km across-track and 18-km along-track radius.

are usually ~ 2 km in magnitude. They may simply be small corrugations due to the influence of older structural fabrics within the underlying Archean or Proterozoic basement.

Images of Venus were produced using a synthetic apperature radar (SAR) which uses time of flight and the Doppler shift to image the surface. Such images are too complicated to interpret in detail. Planes sloping towards the transmitter are foreshortened, whereas those sloping away are dark or in shadow and appear wider than they actually are. The location of imaged objects may be incorrect, particularly where the topography is changing rapidly in space, and objects change their appearance according to the viewing geometry. The images have a horizontal resolution of ~ 100 m. Individual border fault segments in Beta Regio were interpreted using SAR images and topographic profiles determined from altimetric returns.

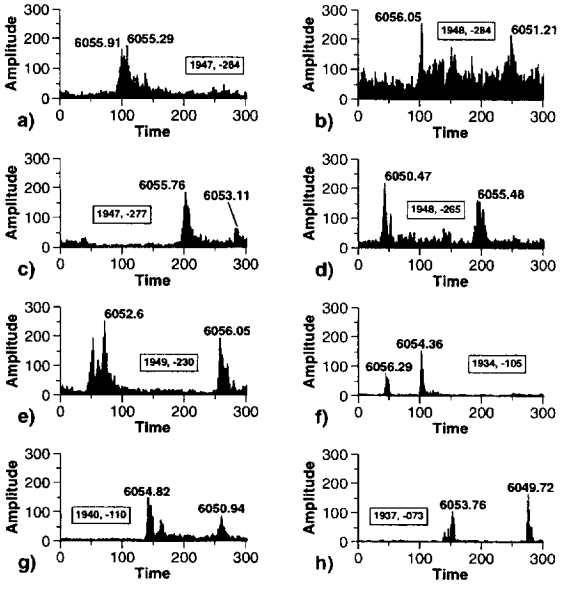

Fig. 4. Doppler-sharpened altimetric radar returns, showing time along the horizontal axis (1 time unit is 224.2 ns) and amplitude of return vertically (arbitrary units). The groundtrack and footprint number of each return is shown. Sharp returns are marked with the absolute altitude (in km) of the topography causing that return. The location of each footprint is shown in Fig. 6 relative to the topographic profiles. The locations of (a), (b) and (c) are shown in Fig. 3. The double peaks in each return are due to energy returned from the top and bottom of the topographic steps which the footprints straddle (see Fig. 6). (a) Orbit no. 1947, footprint no. -284. (b) Orbit no. 1948, footprint no. -284. (c) Orbit no. 1947, footprint no. -277. (d) Orbit no. 1948, footprint no. -265. (e) Orbit no. 1949, footprint no. -230. (f) Orbit no. 1934, footprint no. -105. (g) Orbit no. 1940, footprint no. -110. (h) Orbit no. 1937, footprint no. -073.

Fig. 3a is part of a SAR image (F-MIDR-30N281) of an area of Devana Chasma showing dark and light lineaments. On the basis of their morphology and the distinct topographic step seen across some of these lineations (see below), they are interpreted as scarps caused by faulting, though the imaged planes themselves may be talus slopes. Fig. 3b is a line drawing of the same area, showing those scarps across which it is possible to determine a sense of movement. There is one large, east-dipping plane (Y–Z) in the centre of the image which appears to be imaged, rather than being in shadow, since lineations are visible on the plane. These lineations are not likely to be correctly placed on the image due to the rapidly changing topography. The top and bottom of the surface of this plane are generally clearly defined and the displacement between them dies away along-strike from the centre, reaching zero at points Y and Z. Hence we interpret this plane as one individual fault segment of length ~ 130 km.

West-dipping faults imaged by east-looking radar appear very foreshortened, but there is no danger of the scarp base being obscured by shadows. Hence, there is more certainty that such faults are continuous. An example of a west-dipping fault can be seen (labelled X) in Fig. 3b. This fault is clearly continuous for at least 50 km. Investigation of the area covered by the C1-MIDR-30N279 image revealed at least 14 east-dipping and 4 west-dipping rift-related faults of segment length greater than 50 km.

Fault scarps can also be identified by the topographic step across them. The Magellan spacecraft determined topography by examining the radar returns (echoes) from elliptical areas of the surface (the 'footprint'). Fig. 3b shows the footprints for three altimetry points, and Fig. 4a–c show the corresponding radar returns, plotting signal amplitude against time delay. The time delay of the peak amplitude point is generally used to calculate the surface height, with the sharpness of the peak indicating how rough the terrain is.

Fig. 4a shows a strong echo from the undeformed area west of the rift; the double peak is probably due to slight roughness in terrain and introduces an un-

certainty of ±150 m in height, typical of the uncertainty away from highly deformed areas. Fig. 4b is a return from the edge of the scarp Y–Z and shows two rather weak echoes. It is likely that one is from the rift flank and one from the rift floor, in which case the vertical distance between the two is as much as ~ 5 km. Fig. 4c shows a return from further south with a clear double echo. This suggests that the topographic step of ~ 2.7 km is smaller than that obtained from Fig. 4b. The height of the topographic step may be less than the original total fault throw if there has been subsequent volcanism infilling the rift. The altimetry data therefore suggest that the scarp Y–Z has a maximum vertical displacement of ~ 5 km and that this displacement dies away along-strike, which is consistent with the SAR image interpretation. The existence of additional fault scarps showing vertical offsets of up to 5 km can be inferred from radar returns where the footprints cross these scarps (Fig. 4d–h and Fig. 6a). Hence, the SAR images and altimetric data can be used to infer the presence within Devana Chasma of faults which in terms of both length (up to ~ 100 km) and vertical offset (up to ~ 5 km) are comparable to the scale of East African faults.

4. Maximum half graben widths

The wavelength of half grabens (the distance over which tilting is coherent) in continental rifts is probably related to the effective elastic thickness of the lithosphere in which they form [1,4,5]. The shear stresses required to support the half graben topography decrease with increasing effective elastic thickness. Since the T_e of parts of the East African lithosphere is greater than in most other continental rifts, we may expect wider half grabens for a given shear stress. The structural profiles shown in Fig. 5 show half graben widths of 50 km and more across four rift basins in the southern Western branch of the rift, taken from [8]. These widths are larger than the maximum of ~ 25 km that is common elsewhere in terrestrial continental rifts where T_e is lower [1]. Fig. 5 also shows that the basement throw across some parts of the Western branch may be up to ~ 7 km (profiles A–A′ and D–D′).

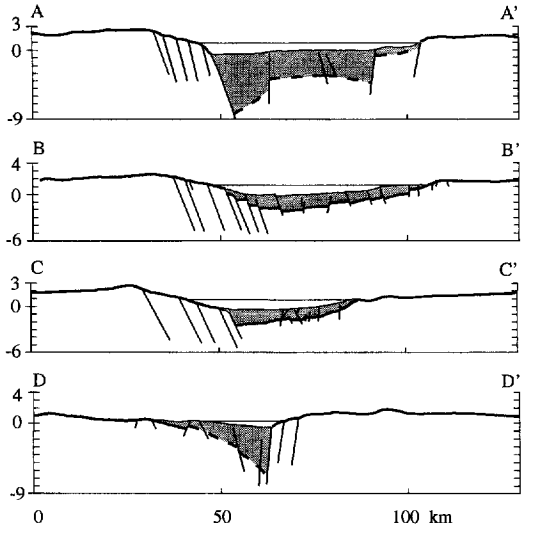

Fig. 5. Structural profiles across the Western branch of the East African Rift System showing sediment-filled (stippled) rift basins bounded by steeply dipping border fault systems, after [29]. Basement topography beneath the sediments is uncertain in sections $A-A'$ and $D-D'$. Basin widths are up to ~ 50 km, with throws on the border faults of up to ~ 7 km. Section lines shown in Fig. 1a. Vertical exaggeration is ~ 2:1.

Profiles across Devana Chasma (Fig. 6a) were obtained by interpolating nearby altimetry points onto the line of profile. Some profiles show pronounced rift-flank uplift, and all show large rift-bounding faults. The apparent low angle of the fault scarps is an artefact of the altimetry point separation (about 30 km). The vertical offset between rift floor and flanks is likely to be underestimated by the profiles because the profiling averages the altimetric measurements taken to either side of the line of the profile. This explains the discrepancy between the vertical step calculated for the large fault above (Y–Z, Fig. 3b; Fig. 4b), and that visible in the profile (B–B′, Fig. 6a). The profiles suggest that the graben width varies from 100 to 200 km, and that the maximum vertical offset is ~ 6 km. It was argued above that topographic steps across some of the Venusian faults may be at least 5 km. This is comparable to the vertical displacement across the entire rift, which is not surprising given that in some places there appear to be only two large faults present. Fig. 6b shows the four African profiles shown in Fig. 5 at the same scale as Fig. 6a. Basement topography has been

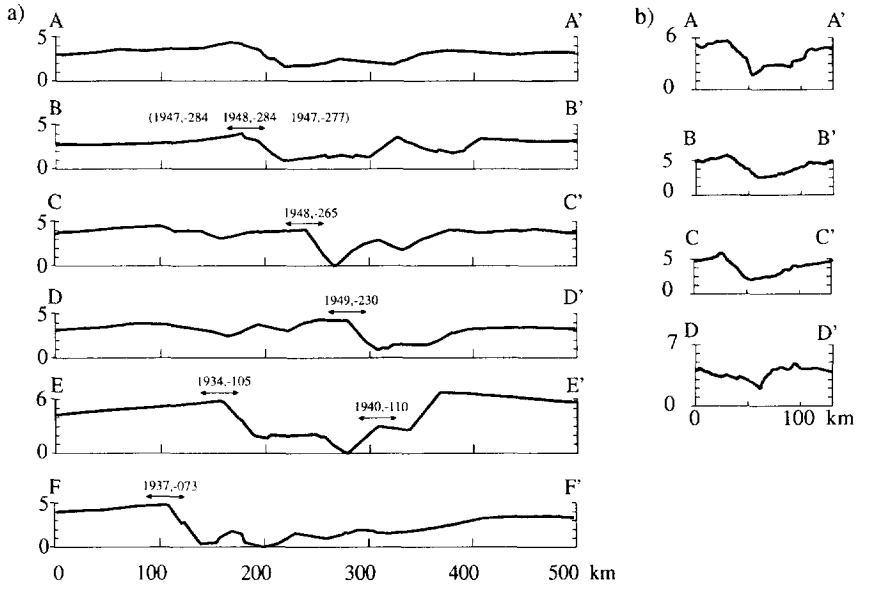

Fig. 6. (a) Topographic profiles across Devana Chasma produced by interpolating nearby altimetric measurements onto the lines of section shown in Fig. 1b. Vertical exaggeration ~ 8:1. Also shown on each profile are the projected positions of the radar altimetry 'footprints' whose returns are shown in Fig. 4. The footprints straddle the topographic steps in the profiles, resulting in energy being returned from both the top and bottom of the steps. (b) Profiles of basement topography for the four East African profiles shown in Fig. 5, drawn to the same vertical and horizontal scale as (a). Basement topography calculated by replacing the water and sediment loads with an equivalent basement load, assuming $\rho_b = 2.9$ Mg m^{-3} and $\rho_s = 2.5$ Mg m^{-3}. Throws on rift-bounding faults are similar to those in Devena Chasma (a), but basin widths are two to three times smaller.

adjusted by replacing water and sediment loads with an equivalent basement load, assuming Airy isostasy, a basement density of 2.9 Mg m^{-3} and a sediment density of 2.5 Mg m^{-3}. This approach is not strictly correct since the lithosphere has been shown to have finite strength. Nevertheless it enables a direct comparison in terms of rift morphology to be drawn between Fig. 6a and Fig. 6b. We do not use the profiles in Fig. 6b to estimate rift dimensions. Vertical displacement of basement across the individual bounding faults in both cases are ~ 5 km, whilst the Venusian rifts are two to three times as wide as those in southern East Africa.

5. Stresses supporting half graben topography

All topography and density contrasts within half grabens are maintained by elastic stresses which are greatest near the bounding faults. We investigate the magnitude of these shear stresses using an extension of McKenzie's method [42]. Note that McKenzie's [42] equation 25 should read:

$$-P_{z=h(1+\xi\cos kx)} + 2\mu\left[\frac{\partial u_z}{\partial_z}\right]_{z=h} = 0 \qquad (1)$$

McKenzie [42] found the maximum resolved shear stress required to support a specified (cosine) topography within a solid elastic layer of thickness T_e overlying a liquid of the same density. Given a more realistic periodic tilted fault block topography we take the Fourier transform, calculate the stress for each wavenumber and then perform the inverse transform to obtain the stress tensor, and hence calculate the maximum resolved shear stress. We specify the topography to be the surface of periodic tilted fault blocks of peak to peak width λ and initial fault dip 60°, with a maximum vertical displacement from the mean level of h and a basement density of ρ_b (Fig. 7a). The hanging wall of each fault is filled with sediments of density ρ_s to a depth h_s. The fill,

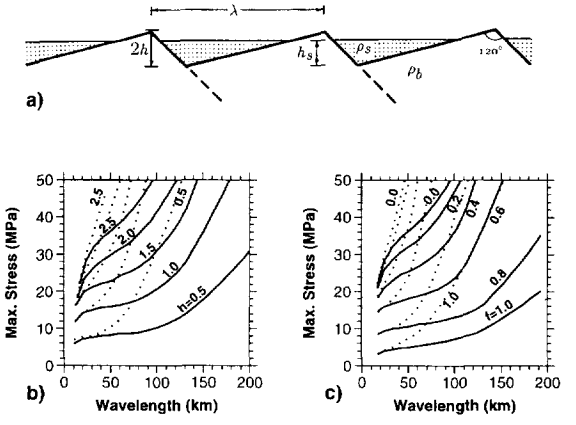

Fig. 7. (a) Geometry of tilted, periodic fault blocks of wavelength λ, initial fault dip of 60° and maximum vertical displacement $2h$. The basement is of density ρ_b and the fault blocks are filled with sediment of density ρ_s to a level h_s. The fill, f, is defined as $h_s/2h$. (b) Effect of varying h and λ on the maximum resolved shear stress for a T_e of 15 km (dotted lines) and 30 km (solid lines). (c) Effect of varying f and λ on the maximum resolved shear stress for a T_e of 15 km (dotted lines) and 30 km (solid lines).

f, of the hanging wall is defined as $h_s/2h$ (Fig. 7a).

We do not use a 'shape-fitting' approach to estimate T_e from the topography. We investigate an entirely different problem and calculate the elastic stresses which are required to support the topography given a particular elastic thickness. The magnitude of these shear stresses increases with the width of the half graben (λ), the vertical displacement on the bounding faults ($2h$) and with the magnitude of the density contrast across the bounding fault. However, they decrease as the effective elastic thickness of the lithosphere increases [1,42]. Wide half grabens require smaller shear stresses to support them if they form in thick elastic sheets rather than thin ones.

Fig. 7b and c show the maximum shear stresses needed to support periodic fault blocks as a function of λ, for varying T_e, h and f. Fig. 7b illustrates how h affects the stresses for $f = 0$ and a T_e of 15 km and 30 km. As h increases from 0.5 km to 2.0 km (equivalent to an increase in vertical offset of the basement of 1.0 to 4.0 km) the stresses increase, for any given λ. Topography supported by an elastic layer of 30 km requires smaller stresses than that of a 15 km thick layer. Fig. 7c shows the effect of varying f from 1.0 (hanging wall full of sediments) to 0 (no sediment infill) for $h = 2.5$, $\rho_s = 2.5$ Mg m^{-3}, and with a T_e of 15 km and 30 km. For a thicker elastic layer the stresses required are less than for a thinner layer.

A number of authors (e.g. [1,4,5]) have suggested that the maximum width of continental half grabens is dependent on the effective elastic thickness of the lithosphere and the maximum shear strength of the bounding faults. Given that the typical stress drop seen in continental earthquakes is in the range 1–10 MPa (10–100 bars) [43] we can calculate the elastic stresses supporting the half grabens for a range of wavelengths, throws and elastic thicknesses. If these elastic stresses exceed ~ 10 MPa, we would expect movement on the faults to reduce the stress.

Fig. 8 shows how the elastic stresses calculated using the periodic fault block model vary with elastic thickness and wavelength of topography for East African and Venusian grabens, using values of h and f that are typical of those rifts (Figs. 5 and 6a). We also show the stresses obtained by approximating the fault block topography to a cosine curve [1], where the amplitude of the cosine curve is calculated such that the area of material above the mean level is equal to that for the fault block, since the stresses are primarily controlled by the mass contrast between the hanging wall fill and the basement. Fig. 8a shows the stresses calculated for East African Rift basins, modelled as periodic fault blocks, using values of $g = 9.8$ m s^{-2}, $\rho_b = 2.9$ Mg m^{-3}, $\rho_s = 2.5$ Mg m^{-3}, $f = 0.8$ and $h = 2.5$ km. The value of stress at which the curves for different values of T_e converge is dependent on h and f (Fig. 7b and c). For the cosine approximation the topography is filled with sediments to the same level as for the fault block model ($f = 0.8$). Fig. 8b shows the Venusian calculations using $g = 8.9$ m s^{-2}, $\rho_b = 2.9$ Mg m^{-3}, no infill ($f = 0$) and $h = 2.5$ km. The calculated stresses differ from those calculated for Africa mainly because of the greater topography on Venus.

From Fig. 5 typical values of λ, h and f in East Africa are 50 km, 2.5 km and 0.8. Fig. 8a shows that using these values the stress required to support such topography, with a T_e of 10 km, is ~ 25 MPa. For a T_e of 30 km (comparable with values obtained for rifted East African lithosphere [12,27–30]) the stress required is ~ 10 MPa. Thus, in East Africa, 50 km wide half grabens can be supported without requiring

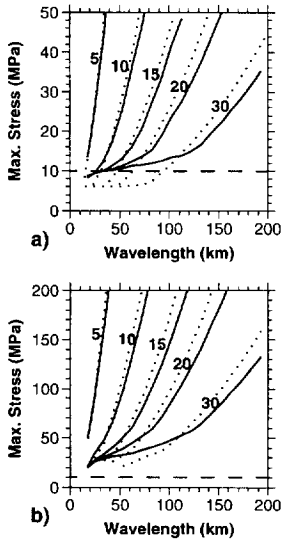

Fig. 8. The variation of maximum resolved shear stress as a function of wavelength and elastic thickness using both the cosine approximation of Jackson and White [1] (dotted lines) and the periodic fault block geometry of Fig. 7a (solid lines) (see text). Paired lines are the cosine and fault block solution for the elastic thickness (T_e) shown between each pair. The dashed line shows the typical maximum stress drop observed in earthquakes on Earth (10 MPa). (a) Results using typical East African values: $g = 9.8$ m s^{-2}, $\rho_b = 2.9$ Mg m^{-3}, $\rho_s = 2.5$ Mg m^{-3}, $f = 0.8$ and $h = 2.5$ km. (b) Results using Venusian values: $g = 8.9$ m s^{-2}, $\rho_b = 2.9$ Mg m^{-3}, no infill and $h = 2.5$ km. For both East Africa and Venus the cosine approximation stresses were calculated by equating the area of the cosine topography above the mean level with that above the mean in the fault block model. Maximum resolved shear stresses were calculated by filling the cosine topography with the same sediment thickness as for the fault block model ($f = 0.8$ for East Africa and 0 for Venus).

shear stresses on the bounding faults that are significantly greater than the stress drops seen in continental earthquakes.

Devana Chasma is wider than most parts of the East African Rift (Figs. 5 and 6). Fig. 8b shows that for an elastic thickness of 30 km, a topographic step of 5 km and a rift width of 150 km (see Fig. 6a), the stresses required to support the topography are ~ 80 MPa. This is considerably greater than the stress drop observed in normal-faulting earthquakes on Earth, and arises from the greater width of the graben and the greater density contrast across the bounding faults. This suggests that Venusian faults can withstand greater stresses than those in East Africa, even though the elastic thickness of the lithosphere is similar in both cases. If Venusian faults were no stronger than those on Earth then the observed topography could not be supported elastically. If we have overestimated the width of Venusian grabens by a factor of two, then the shear stress required is reduced to ~ 40 MPa. This is still greater than the typical earthquake stress drops seen on Earth.

6. Discussion

The rift systems of southern East Africa and Beta Regio are remarkably similar in a number of ways. Within rifted areas, the effective elastic thickness in each case is ~ 30 km, suggesting that both lithospheres maintain significant strength during rifting. The large T_e of the Venusian lithosphere is interesting because the surface temperature is about 450°C. It has been suggested that on Earth the depth to the 450°C isotherm approximates the elastic thickness for oceanic and continental lithosphere [24,44]. Given that the surface of Venus approximates a basaltic composition, it seems that the absence of water greatly increases the near-surface strength of the lithosphere [45]. Hence a large T_e can be maintained despite the surface temperature. Similarly, because of the high surface temperatures we would not expect brittle deformation to occur on Venus if the near-surface rheology were the same as on Earth. Since we do see extensive surface faulting, we conclude that the near-surface rheology must differ from that of the Earth. The faults bounding the rifts on both planets have a maximum length scale of ~ 100 km, with throws across such faults being ~ 2–7 km. It is interesting that the maximum fault segment length seen in southern East Africa is two or three times the seismogenic thickness, in contrast to faults seen in other extensional areas where the maximum fault length is approximately equal to the down-dip fault width [1].

The southern East African and Beta Regio rift systems differ in their widths. Parts of southern East Africa have maximum half graben widths of ~ 50 km, whilst Beta Regio grabens are ~ 150 km wide. Such a difference in maximum widths may be significant. The elastic thicknesses of both southern East Africa and Beta Regio are similar, and therefore the

greater width of the graben and absence of sediment fill on Venus requires the shear stresses supporting the topography to be greater than in East Africa. It seems plausible to suggest that the bounding faults on Venus may be stronger than in East Africa, and are therefore able to accommodate greater shear stresses before slip occurs. If they are not stronger than faults on Earth then the topography observed could not be supported elastically. Faults on Earth are weak zones [46] and the $\sim 1-10$ MPa stress drop seen in earthquakes may be close to the total shear stress acting on the faults. This poses an interesting problem; how can faults be weak on Earth and strong on Venus, even though Venus is hotter? One possible explanation may be the absence of water on Venus. On Earth, it is suggested that over-pressured pore fluid within a fault gouge may lubricate the fault and reduce the total frictional stress acting on it [47]. It is not clear that fluid pressure does reduce the frictional stress in such a way, but if it does then faults on Venus cannot be lubricated in this way. Drawing yield strength envelopes even for Earth is problematic; despite their popularity such curves cannot account for the constant stress drop seen in earthquakes at all depths. On Venus we have even less information regarding rheology and stresses at depth.

7. Conclusions

The purpose of this paper was to show that parts of the rift systems of East Africa and Beta Regio, Venus are similar in several respects. Both rift systems have effective elastic thicknesses of ~ 30 km and maximum fault segment lengths of ~ 100 km. However, the rift systems differ in their maximum widths. The wider rifts seen on Venus suggest that the faults bounding Venusian rifts are stronger than faults on Earth. We attribute the greater lengths of fault segments and greater widths of half grabens in East Africa, compared to other actively extending regions, to the presence of cold lithosphere. We have little information on the rheological properties of the Venusian lithosphere, but we suggest that the absence of water on the planet may increase the strength of the uppermost lithosphere and of the faults. If the stresses due to convective mantle circulation on the two planets are of approximately the same magnitude, the fact that much greater stresses are required to cause fault movement on Venus than on Earth may explain why large scale plate tectonics are not currently seen on Venus.

Acknowledgements

We thank the Tanzanian Commission for Science and Technology for permission to work in Tanzania. Discussions with Dan McKenzie, James Jackson, Cindy Ebinger and Nicky White greatly improved this paper, as did the comments of three anonymous referees. Financial support for this work was provided by N.E.R.C. (Studentship GT4/93/133/G to AF), Shell International Petroleum Company U.K. (Studentship to FN), The Royal Society and Amerada Hess. Department of Earth Sciences Contribution No. 4726. *[PT]*

References

[1] J.A. Jackson and N.J. White, Normal faulting in the upper continental crust: observations from regions of active extension, J. Struct. Geol. 11, 15–36, 1989.

[2] J.A. Jackson and T. Blenkinsop, The Malawi earthquake of March 10, 1989: deep faulting within the East African rift system, Tectonics 12, 1131–1139, 1993.

[3] N.J. Hayward and C.J. Ebinger, Variations in the along axis segmentation of the Afar Rift System, Tectonics 15, 244–257, 1996.

[4] G.C.P. King, R.S. Stein and J.B. Rundle, The growth of geological structures by repeated earthquakes, 1. Conceptual framework, J. Geophys. Res. 93, 13,307–13,318, 1988.

[5] R.S. Stein, G.C.P. King and J.B. Rundle, The growth of geological structures by repeated earthquakes, 2. Field examples of continental dip-slip faults, J. Geophys. Res. 93, 13,319–13,331, 1988.

[6] G. WoldeGabriel, J.L. Aronson and R.C. Walter, Geology, geochronology, and rift basin development in the central sector of the Main Ethiopia Rift, Geol. Soc. Am. Bull. 102, 439–458, 1990.

[7] C.J. Ebinger, A.L. Deino, A.L. Tesha, T. Becker and U. Ring, Tectonic controls on rift basin morphology: evolution of the Northern Malawi (Nyasa) rift, J. Geophys. Res. 98, 17,821–17,836, 1993.

[8] C.J. Ebinger, Tectonic development of the Western branch of the East African rift system, Geol. Soc. Am. Bull. 101, 885–903, 1989.

[9] C.J. Ebinger, Geometric and kinematic development of border faults and accommodation zones, Kivu–Rusizi rift, Africa, Tectonics 8, 117–133, 1989.

[10] F. Jestin, P. Huchon and J.M. Gaulier, The Somali plate and the East African rift system: present-day kinematics, Geophys. J. Int. 116, 637–654, 1994.
[11] J. Fairhead, Structure of the lithosphere beneath the Eastern rift, East Africa, deduced from gravity studies, Tectonophysics 30, 269–298, 1976.
[12] C.J. Ebinger, T.D. Bechtel, D.W. Forsyth and C.O. Bowin, Effective elastic plate thickness beneath the East African and Afar plateaus and dynamic compensation of the uplifts, J. Geophys. Res. 94, 2883–2901, 1989.
[13] G.S. Wagner and C.A. Langston, East African body wave inversion with implications for continental structure and deformation, Geophys. J. Oxford 94, 503–518, 1988.
[14] A.A. Nyblade and C.A. Langston, East African earthquakes below 20 km and their implications for crustal structure, Geophys. J. Int. 121, 49–62, 1995.
[15] A. Foster, J. Jackson and C. Ebinger, Source mechanisms and centroid depths of East African earthquakes; implications for rifting of old, cold lithosphere, EOS Trans. AGU 76, 639, 1995.
[16] J. Deverchere, F. Houdry, N.V. Solonenko, A.V. Solonenko and V.A. Sankar, Seismicity, active faults and stress field of the north Muya Region, Baikal Rift: new insights on the rheology of extended continental lithosphere, J. Geophys. Res. 98, 19,895–19,912, 1993.
[17] P.K.H. Maguire, C.J. Swain, R. Masotti and M.A. Khan, A crustal and uppermost mantle cross-sectional model of the Kenya Rift derived from seismic and gravity data, Tectonophysics 236, 217–249, 1994.
[18] G.E. McGill, S.J. Steenstrup, C. Barton and P.G. Ford, Continental rifting and the origin of Beta Regio, Venus, Geophys. Res. Lett. 8, 737–740, 1981.
[19] D.A. Senske, G.G. Schaber and E.R. Stofan, Regional topographic rises on Venus: geology of Western Eistla Regio and comparison to Beta Regio and Atla Regio, J. Geophys. Res. 97, 13,395–13,420, 1992.
[20] Yu.A. Surkov, V.L. Barsukov, L.P. Moskalyova, V.P. Kharyukova and A.L. Kemurdzhian, New data on the composition, structure and properties of Venus rock obtained by Venera 13 and 14, Proc. Lunar Planet. Sci. Conf. 14th, Part 2, J. Geophys. Res. 89, Suppl., B393–B402, 1984.
[21] E.B. Burov and M. Diament, The effective elastic thickness (T_e) of continental lithosphere: what does it really mean? J. Geophys. Res. 100, 3905–3927, 1995.
[22] S. Cloetingh and E.B. Burov, Thermomechanical structure of European continental lithosphere: constraints from rheological profiles and EET estimates, Geophys. J. Int. 124, 695–723, 1996.
[23] G.D. Karner, M.S. Steckler and J.A. Thorne, Long-term thermo-mechanical properties of the continental lithosphere, Nature 304, 250–253, 1983.
[24] P.J. Barton and R. Wood, Tectonic evolution of the North Sea basin: crustal stretching and subsidence, Geophys. J.R. Astron. Soc. 79, 987–1002, 1984.
[25] S. Fowler and D. McKenzie, Flexural studies of the Exmouth and Rockall plateaux using SEASAT altimetry, Basin Res. 2, 27–34, 1989.
[26] T.D. Bechtel, D.W. Forsyth, V.L. Sharpton and R.A.F. Grieve, Variations in effective elastic thickness of the North American lithosphere, Nature 343, 636–638, 1990.
[27] D.W. Forsyth, Subsurface loading and estimates of the flexural rigidity of the continental lithosphere, J. Geophys. Res. 90, 12,623–12,632, 1985.
[28] T.D. Bechtel, D.W. Forsyth and C.J. Swain, Mechanisms of isostatic compensation in the vicinity of the East African Rift, Kenya, Geophys. J.R. Astron. Soc. 90, 445–465, 1987.
[29] C.J. Ebinger, G.D. Karner and J.K. Weissel, Mechanical strength of extended continental lithosphere: constraints from the Western rift system, East Africa, Tectonics 10, 1239–1256, 1991.
[30] N.M. Upcott, R.K. Mukasa, C.J. Ebinger and G.D. Karner, Along-axis segmentation and isostasy in the Western rift, East Africa, J. Geophys. Res. 101, 3247–3268, 1996.
[31] D. and C. Bowin, The relationship between bathymetry and gravity in the Atlantic Ocean, J. Geophys. Res. 81, 1903–1915, 1976.
[32] D. and F. Nimmo, Elastic thickness estimates for Venus from line of sight accelerations, Icarus, submitted 1995.
[33] S.E. Smrekar, Evidence for active hotspots on Venus from analysis of Magellan gravity data, Icarus 112, 2–26, 1994.
[34] R.J. Phillips, Estimating lithospheric properties at Atla Regio, Venus, Icarus 112, 147–170, 1994.
[35] D.P. Schwartz and K.J. Coppersmith, Fault behaviour and characteristic earthquakes: examples from the Wasatch and San Andreas fault zones, J. Geophys. Res. 89, 5681–5698, 1984.
[36] A.J. Crone and K.M. Haller, Segmentation and coseismic behaviour of basin-and-range normal faults: examples from east-central Idaho and southwestern Montana, U.S.A., J. Struct. Geol. 13, 151–164, 1991.
[37] C.J. Ebinger, M.J. Crow, B.R. Rosendahl, D.A. Livingstone and J. LeFournier, Structural evolution of Lake Malawi, Africa, Nature 308, 627–629, 1984.
[38] W.H. Wheeler and J.A. Karson, Extension and subsidence adjacent to a 'weak' continental transform: an example from the Rukwa rift, East Africa, Geology 22, 625–628, 1994.
[39] E.A. Kilembe and B.R. Rosendahl, Structure and stratigraphy of the Rukwa rift, Tectonophysics 209, 143–158, 1992.
[40] W.H. Wheeler and B.R. Rosendahl, Geometry of the Livingstone Mountains border fault, Nyasa (Malawi) rift, East Africa, Tectonics 13, 303–312, 1994.
[41] J.B. Dawson, Neogene tectonics and volcanicity in the North Tanzania sector of the Gregory Rift Valley: contrasts with the Kenya sector, Tectonophysics 204, 81–92, 1992.
[42] D. Some remarks on heat flow and gravity anomalies, J. Geophys. Res. 72, 6261–6263, 1967.
[43] C.H. Scholz, Scaling laws for large earthquakes: consequences for physical models, Bull. Seismol. Soc. Am. 72, 1–14, 1982.
[44] A.B. Watts and S.F. Daly, Long wavelength gravity and topography anomalies, Ann. Rev. Earth Planet. Sci. 9, 415–448, 1981.
[45] S.J. Mackwell, M.E. Zimmerman, D.L. Kohlstedt and D.S. Scherber, Experimental deformation of dry Columbia dia-

base: implications for tectonics on Venus, in: Rock Mechanics, Proceedings of the 35th US Symposium, J.J.K. Daemen and R.A. Schultz, eds., pp. 207–214, Balkema, Rotterdam, 1995.

[46] N.H. Sleep and M.L. Blanpied, Creep, compaction and the weak rheology of major faults, Nature 359, 687–692, 1992.

[47] J.R. Rice, Fault stress states, pore pressure distributions, and the weakness of the San Andreas fault, in: Fault Mechanics and Transport Properties of Rocks, B. Evans and T-F. Wong, eds., pp. 475–503, Academic, San Diego, CA, 1992.